

Desynchronized wave patterns in synchronized chaotic regions of coupled map lattices

P. Palaniyandi, P. Muruganandam, and M. Lakshmanan

*Centre for Nonlinear Dynamics, Department of Physics,
Bharathidasan University, Tiruchirapalli 620 024, India*

(Dated: December 2, 2024)

We analyze the size limits of coupled map lattices at the crossover of low dimensional to high dimensional chaos. We find an interesting class of standing wave type periodic patterns, within the low dimensional limit, in addition to the stable synchronous chaotic states depending upon the initial conditions. Further, we bring out a controlling mechanism to explain the emergence of standing wave patterns in the coupled map lattices. Finally, we give an analytic expression in terms of the unstable periodic orbits of the isolated map to represent the standing wave patterns.

PACS numbers: 05.45.Ra, 05.45.Xt

I. INTRODUCTION

Coupled dynamical systems often arise in nature whenever a collective or cooperative phenomenon is favoured. Such coupled systems are very useful in modeling spatially extended dynamical systems in physical, biological, ecological and social sciences [1, 2, 3, 4, 5]. In general, these systems can be visualized as a collection of large number of low dimensional systems, either identical or different in nature, appropriately coupled (locally or globally) to each other. In most cases it happens that these systems evolve in synchrony with each other. Examples include synchronized flashing of fire flies, classic observation of Huygens on pendulum clocks, etc. [2]. In this context, studies on synchronization in coupled systems has been given a central importance for the past two decades in chaotic dynamics [6, 7, 8].

In particular, the coupled map lattice (CML) provides a prototype model to study various features associated with the cooperative evolution of constituent systems [9, 10, 11]. They occur in a variety of fields involving spatiotemporal complexity [12]. One of the important properties of CML is that they exhibit size instability, that is, there is a limit in the number of constituents for which stable synchronous chaotic state exists. Increasing the number of constituents beyond this limit (critical size) leads to the occurrence of spatially incoherent behaviour (eg. high dimensional chaos). For example, Bohr and Christensen [13] have studied such size instability behaviour in a two dimensional coupled logistic lattice. Similar desynchronization has been found in arrays of coupled systems represented by nonlinear oscillators [4, 14, 15, 16]. The stability of synchronous chaos in coupled dynamical systems plays an important role in the study of pattern formation, spatiotemporal chaos, etc. [4, 13, 14, 17, 18].

In general, these studies on size instability are valid in most situations. However, we find that in certain circumstances there is an ambiguity in dealing with these systems below the critical system sizes. To be specific, there exist certain ranges of initial conditions for which the CML admits spatially and temporally periodic type solutions in contrast to the usually expected stable syn-

chronous chaos. The central theme of this paper is to study such periodic states (standing wave type) that co-exist with the stable synchronous chaotic state well below the critical system size. In this paper, we explain the presence of standing wave solutions using a type of control mechanism and present their connection with the unstable periodic orbits (UPOs) of isolated maps qualitatively. In particular, UPOs are essentially the building blocks of any chaotic attractor, which is embedded with an infinite number of such UPOs. In fact, we point out how the UPOs of isolated chaotic systems can play a crucial role in the formation of standing wave patterns in CMLs.

The structure of the paper is as follows. In Sec. II, we present a rather brief overview on the size instability in coupled map lattices (CMLs) and illustrate it numerically using coupled logistic lattice (CLL). Then, in Sec. III we point out that CML exhibits standing wave type solutions in addition to the expected stable synchronous states within the critical system size limit. We describe a type of controlling mechanism which explains the emergence of standing wave type patterns in Sec. IV. Further, in Sec. V, we propose a simple analytical expression for the standing wave patterns which often emerge in the CML in terms of the UPOs of isolated maps. Finally, in Sec. VI, we present a the summary and conclusion.

II. SIZE INSTABILITY IN COUPLED MAP LATTICES

Consider an one dimensional identically coupled map lattice with nearest neighbour coupling [9]

$$x_{n+1}^j = f(x_n^j) + \epsilon [f(x_n^{j-1}) + f(x_n^{j+1}) - 2f(x_n^j)], \quad (1)$$

where j ($= 0, 1, 2, \dots, L - 1$) represents the lattice sites and L is the system size, subject to periodic boundary conditions.

The main goal of this section is to study the stability of the synchronized chaotic state defined by $s_n = x^0 = x^1 = \dots = x^{L-1}$ in diffusively coupled map lattices using the procedure derived originally for coupled oscillators in

the case of shift-invariant coupling by Heagy *et al* [14]. The linearization of the above CML about the synchronized chaotic state s_n leads to a set of linear variational equations given by

$$\begin{aligned}\xi_{n+1}^j &= Df(s_n)\xi_n^j + \epsilon \left[D_{j-1}f(x^{j-1}) \Big|_s \xi_n^{j-1} \right. \\ &\quad \left. + D_{j+1}f(x^{j+1}) \Big|_s \xi_n^{j+1} - 2D_j f(x^j) \Big|_s \xi_n^j \right],\end{aligned}\quad (2)$$

where $\xi^j = x^j - s_n$ and D_j are the differential operators acting on j -th map in the CML. Since the system under study is shift invariant, all the coupling functions can be expressed in terms of the coupling function of the first map as

$$\begin{aligned}\xi_{n+1}^j &= Df(s_n)\xi_n^j + \epsilon \left[D_{L-1}f(x^{L-1}) \Big|_s \xi_n^{j-1} \right. \\ &\quad \left. + D_1f(x^1) \Big|_s \xi_n^{j+1} - 2D_0f(x^0) \Big|_s \xi_n^j \right].\end{aligned}\quad (3)$$

Eq. (3) can be rewritten in the form of a discrete circular convolution after defining a sequence

$$H^L = Df(s) - 2\epsilon D_0f(x^0) \Big|_s \equiv H^0,\quad (4a)$$

$$H^{L-1} = \epsilon D_{L-1}f(x^{L-1}) \Big|_s \equiv H^{-1},\quad (4b)$$

$$H^{L+1} = \epsilon D_1f(x^1) \Big|_s \equiv H^1\quad (4c)$$

as

$$\xi_{n+1}^i = \sum_{j=i-1}^{i+1} H^{j-i} \xi_n^j, \quad i = 0, 1, 2, \dots, L-1.\quad (5)$$

By introducing discrete Fourier transforms for sequences H^j and ξ^j ,

$$Y^k = \frac{1}{\sqrt{L}} \sum_{j=L-1}^{L+1} H^j e^{2\pi i j k / L}\quad (6a)$$

$$\eta^k = \frac{1}{\sqrt{L}} \sum_{j=L-1}^{L+1} \xi^j e^{2\pi i j k / L}, \quad k = 0, 1, \dots, L-1\quad (6b)$$

and using the convolution theorem for discrete Fourier transforms [19] the transformed variational equations are given by

$$\eta_{n+1}^k = \sqrt{L} Y^k \eta_n^k.\quad (7)$$

The transformed basis η^k decomposes the variations into variation within and variation transverse to the synchronization manifold defined by $x^0 = x^1 = \dots = x^{L-1}$. From (6b) one can infer that the vector η^0 is the variation on the synchronization manifold and η^k , $k = 1, 2, \dots, L-1$, are the transformed variations transverse to the synchronization manifold. By substituting Eq. (6a) in Eq. (7) we get

$$\begin{aligned}\eta_{n+1}^k &= \left[Df(s) - 2\epsilon D_0f(x^0) \Big|_s \right. \\ &\quad \left. + \epsilon D_{L-1}f(x^{L-1}) \Big|_s e^{-2\pi i k / L} \right. \\ &\quad \left. + \epsilon D_1f(x^1) \Big|_s e^{2\pi i k / L} \right] \eta_n^k, \quad k = 1, 2, \dots, L-1\end{aligned}\quad (8)$$

On the synchronization manifold $x^0 = x^1 = \dots = x^{L-1} = s_n$, we have

$$D_0f(x^0) \Big|_s = D_1f(x^1) \Big|_s = \dots = D_{L-1}f(x^{L-1}) \Big|_s,\quad (9)$$

the above variational equations become

$$\eta_{n+1}^k = Df(s) \left[1 - 4\epsilon \sin^2 \left(\frac{\pi k}{L} \right) \right] \eta_n^k.\quad (10)$$

From the above one can easily deduce the relation connecting transverse Lyapunov exponents (TLEs), which determines the stability of the synchronous state, in terms of the Lyapunov exponent of single (isolated) map, λ^0 as

$$\lambda^k = \lambda^0 + \ln \left[1 - 4\epsilon \sin^2 \left(\frac{\pi k}{L} \right) \right].\quad (11)$$

The synchronous state is stable only if the TLEs (λ^k , $k = 1, 2, \dots, L-1$) are all negative.

The above relation (11) can also be obtained by means of a direct perturbation of the form

$$x_n^j = s_n + \delta \exp \left(i \frac{2\pi k}{L} \right) \exp(\lambda^k n), \quad \delta \ll 1,\quad (12)$$

as considered by Bohr and Christensen [13].

The synchronous state loses its stability when the long waves (lowest mode) are unstable [13]. This means that for $\lambda^1 > 0$ the synchronous state is unstable. Thus, substituting $\lambda^1 = 0$ in Eq. (11), one obtains the maximum/critical lattice size (L_c) that supports stable synchronous state as

$$L_c = \text{int} \left(\frac{\pi}{\sin^{-1} \left(\sqrt{\frac{1-e^{-\lambda_0}}{4\epsilon}} \right)} \right).\quad (13)$$

Now, let us consider a coupled logistic lattice (CLL) where each lattice site in Eq. (1) is occupied by the logistic map,

$$f(x) = \mu x(1-x), \quad x \in (0, 1), \quad \mu \in (0, 4).\quad (14)$$

In particular for the choice, $\mu = 3.5732$, the Lyapunov exponent of single (isolated) map is positive (*i.e.*, $\lambda^0 \sim 0.057 > 0$) and chaotic. In this case, for coupling strength $\epsilon = 0.2$, the critical lattice size (L_c) is found to be 11 from Eq. (13). One can also verify this value numerically by considering the CLL with random initial conditions and periodic boundary conditions. Figs. 1(a) and 1(b) show the nature of dynamical evolution of the CLL at (synchronous chaos) and above (asynchronous orbit) the critical lattice size, respectively. In Fig. 1(a), the randomly chosen initial state for $L = 11$ is shown to restrict the dynamics to the synchronization manifold, where all the lattices evolve exactly in synchrony with each other. On the other hand, for $L = 12$, [cf. Fig. 1(b)] the synchronization is found to be lost, thereby confirming the size instability in the CLL.

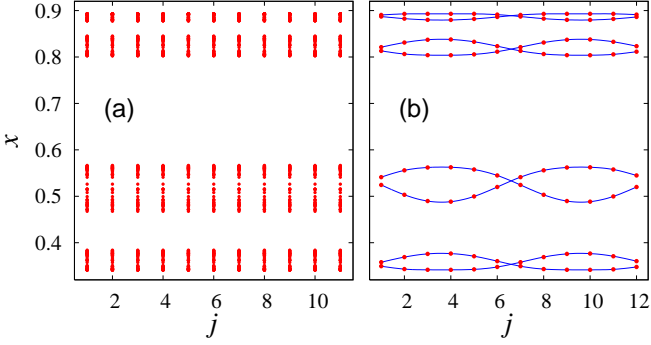


FIG. 1: Dynamics of coupled logistic lattice (1) and (14) (a) for $L = 11$ (synchronized chaos) and (b) $L = 12$ (standing wave type spatiotemporal patterns) for random initial conditions and periodic boundary conditions.

The stability analysis discussed above holds good if the coupled system supports long wave instability. However, in addition, we have found from a detailed numerical analysis of the CLL that there exists a new kind of instability by which the system (1) shows interesting standing wave type patterns (even for $L \leq 11$) to be discussed in the following sections.

III. EXISTENCE OF MULTIPLE STABLE STATES IN COUPLED MAP LATTICES

From the above analysis, it is clear that the coupled map lattice (1) with periodic boundary conditions exhibits synchronous chaos up to a certain critical lattice size (L_c). However, the dynamics is often dependent on the choice of the initial conditions. In order to understand the role of the initial conditions, we again consider coupled logistic lattice (CLL) with the same parameters as used in the previous section ($\mu = 3.5732$ and $\epsilon = 0.2$ in Eqs. (1) and (14)).

When random initial conditions are assumed, in most cases, CLL exhibits stable synchronous chaos for $2 \leq L \leq 11$ as predicted by Eq. (13). However, there are certain ranges of initial conditions for which CLL shows some interesting asynchronous spatiotemporal patterns even for $L < L_c$. For example, for $L = 8$ and with the choice of initial conditions $\{x_0^j\}_{j=0}^{L-1} = \{0.1, 0.01, 0.7, 0.2, 0.65, 0.1, 0.15, 0.001\}$ or several nearby initial conditions, the CLL exhibits a standing wave type pattern as shown in Fig. 2(a). But for the same lattice size, if we choose a different set of initial conditions, $\{x_0^j\}_{j=0}^{L-1} = \{0.0004, 0.0001, 0.0003, 0.0005, 0.00045, 0.00018, 0.00016, 0.00001\}$ or the nearby points, two standing waves with different amplitudes are produced within the CLL as in Fig. 2(b). Similarly a disturbed standing wave pattern as shown in Fig. 2(c) is possible to be exhibited by the CLL for many choices of initial conditions. A synchronous chaos, as one would expect

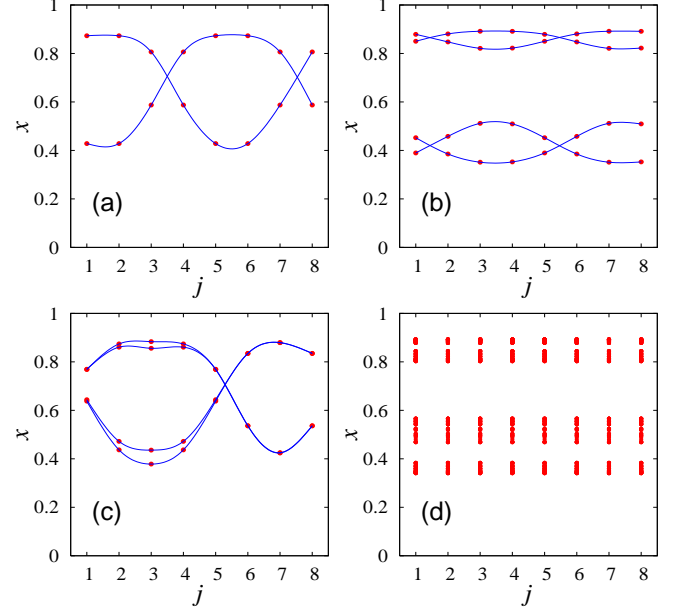


FIG. 2: The possible spatiotemporal patterns in coupled logistic lattice (1) and (14) with $L = 8$ for different initial conditions. (a) single standing wave, (b) double standing waves (c) single standing wave with a temporal period-2 orbit in one half and period-4 orbit in another and (d) synchronized chaos.

TABLE I: The possible spatiotemporal patterns for different lattice sizes and their percentage of occurrence for the coupled logistic lattice sampled over a set of 10^6 random initial conditions (i.c.'s). The parameter are fixed as $\mu = 3.5732$ in Eq. (14) and $\epsilon = 0.2$ in Eq. (1). Here, SW: standing wave, sync.: synchronized.

size (L)	spatiotemporal patterns	% of i.c.'s	size (L)	spatiotemporal patterns	% of i.c.'s
6	single SW	9	10	double SWs	43
	sync. chaos	91		sync. chaos	45
7	single SW	22	11	others	12
	sync. chaos	78		double SWs	48
8	single SW	21	12	four SWs	2
	double SWs	10		sync. chaos	34
	sync. chaos	66		others	16
	others	3		double SWs	24
9	double SWs	38	13	four SWs	28
	sync. chaos	54		sync. chaos	0.2
	others	8		others	47.8

for $L = 8$ from the theory, is also exhibited by the CLL as depicted in Fig. 2(d), for most of the random choices of initial conditions. This kind of multiple stable solutions is also observed in the CLL for other lattice sizes, namely $L = 6, 7, 9$ and 10 which are also less than L_c . The occurrence of various spatiotemporal patterns for different lattice sizes of the CLL and their percentage of occurrence

are shown in Table I. In order to quantify the percentage of occurrence of different spatiotemporal patterns, we have used 10^6 sets of random initial conditions (i.c.'s) in the interval 0 to 1 and identified the number of i.c.'s which lead to a specific pattern as indicated in Table I. We have further confirmed our assertion by analyzing the same systems in different computing environments such as Intel Pentium 4, Sun Sparc server/workstation and Compaq Alpha workstation.

The above results confirm the coexistence of synchronized chaos and standing wave patterns in the CML having lattice size even much smaller than L_c according to the choice of initial conditions. In other words, there exists multiple stable solutions to the CML for a particular set of values of the parameters depending on the initial state of the constituents. This implies that apart from the long wave instability, certain other mechanisms are involved in driving the CML to exhibit the regular standing wave patterns. We discuss their origin in the following section.

IV. EMERGENCE OF STANDING WAVE PATTERNS BY CONTROLLING

The extraordinary behaviour of the CML showing standing wave patterns well below the critical lattice size (L_c) can be explained as follows. The effect of coupling part, that is, the second term in the right hand side of Eq. (1), can be considered as a kind of force or perturbation applied to every lattice point in the CML and we call it as the coupling force. In fact this force on a particular lattice point is developed either due to a mismatch in the parameters of the neighbouring lattice points or due to differences in their initial conditions or both. If the neighbouring lattice points are identical then this force is formed due to variation in the initial conditions and our system indeed falls under this category. In general, the strength of the coupling force at all the lattice points approaches zero when they oscillate towards synchronization with their neighbours, and usually this will happen for $L \leq L_c$. But in the case of $L > L_c$, this force at every lattice point oscillates periodically or in a chaotic manner, giving rise to various spatiotemporal patterns, including standing waves. However, as we have pointed out above that under certain circumstances, (*i.e.*, for certain ranges of initial conditions), even for $L < L_c$, the coupling force of each and every lattice point oscillates periodically with different amplitudes and thereby makes the CML to exhibit spatiotemporal periodic (standing wave) solutions. In general, the periodic oscillations in the coupling force may be of any period and this fixes the number of standing waves produced within the lattice. A careful analysis from our numerical studies shows that if p is the period of oscillation in the coupling force then $p/2$ different standing waves are formed within the lattice as explained below.

In order to understand the mechanism behind the

emergence of spatiotemporal periodic structure, let us now consider a specific case of the periodically oscillating coupling force of period two, that is, the force oscillating between two fixed amplitudes, say, k_1 and k_2 so that a single standing wave is formed in the CML. Then the amplitudes of the coupling force at the j^{th} lattice site will alternate between the numerical values k_1^j and k_2^j , where $j = 1, 2, \dots, L$. Thus, the evolution of j^{th} map in the CML can be effectively described by the equation

$$\begin{aligned} x_{n+1}^j &= f(x_n^j) + k_1^j, \\ x_{n+2}^j &= f(x_{n+1}^j) + k_2^j. \end{aligned} \quad (15)$$

For a given lattice point j , this is nothing but a single logistic map with a periodic kick of period-2 (modified map). It is now obvious to note from Eqs. (15) and (1) that the original coupled map lattice exhibiting a standing wave pattern can be decomposed into L number of modified maps such that the dynamics of (1) is essentially mimicked by the set (15). We call the decoupled map as a modified map because the nature of evolution of this map is different from that of original constituent map ($x_n^j = f(x_{n-1}^j)$) of the CML even though their Jacobian matrix and parameters are the same. Thus studying the evolution of L decoupled modified maps (15) with allowed sets of values for k_1^j and k_2^j is equivalent to that of the original CML, given by Eq. (1).

The inclusion of suitable external forces (constant or periodic) into the evolution equation of a dynamical system may lead to qualitative changes in its dynamics [3] and this procedure can be considered as a kind of controlling. For example, a chaotically evolving system can be controlled to a stable periodic orbit by the addition of an appropriate constant or periodic external bias [3, 20, 21]. As a consequence, one can visualize the present problem as a kind of controlling and expect a stable fixed point solution for the modified map (15) for appropriate forcing amplitudes (k_1 and k_2), with same set of parameters for which the original map, $x_n^j = f(x_{n-1}^j)$, exhibits chaotic solution. Thus there exists a possibility for obtaining periodic solutions of period two for *the constituent map within the CML* even though its parameter is in the chaotic region of the individual map. This confirms the occurrence of spatiotemporal periodic structure in the CML with certain allowed values of amplitude of the coupling forces noted below.

In the case of coupled logistic lattice with parameters mentioned in the previous section, the allowed region of forcing amplitudes which lead the decoupled modified map (15) to exhibit period two solution is shown in Fig. 3. For details see Appendix A. For $L = 8$, we have calculated the amplitudes of the coupling force (that is, the second term in the right hand side of Eq. (1)) of period-2 for the initial conditions, $\{x_0^j\}_{j=0}^{L-1} = \{0.1, 0.01, 0.7, 0.2, 0.65, 0.1, 0.15, 0.001\}$, and these are shown in Table II. Now one can easily check that these amplitudes of the coupling force fall in the region specified by the phase diagram shown in Fig. 3. That is, in this case, for a

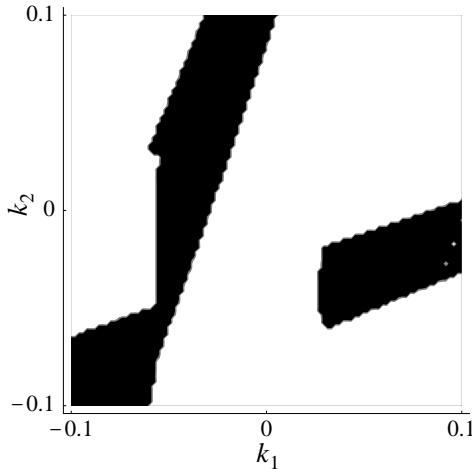


FIG. 3: The phase diagram in the $k_1 - k_2$ plane for the modified map (15) with $f(x) = \mu x(1-x)$, $\mu = 3.5732$, showing the regions which correspond to the periodic solution of period 2 (dark region).

suitable set of initial conditions, the coupling force is set spontaneously in such a way that all the lattice points are oscillating periodically with period two. It may also be noted that from Table II that the numerical values of the forcing amplitudes k_1 and k_2 repeat suitably at different lattice points so as to obtain a standing wave spatially [cf. Fig. 2(a)].

TABLE II: Amplitudes of the coupling force k_1 and k_2 in the coupled map lattices for $L = 8$ with period-2 for initial conditions, $\{x_0^j\}_{j=0}^{L-1} = \{0.1, 0.01, 0.7, 0.2, 0.65, 0.1, 0.15, 0.001\}$.

lattice site(j)	k_1^j ($\times 10^{-2}$)	k_2^j ($\times 10^{-2}$)	lattice site(j)	k_1^j ($\times 10^{-2}$)	k_2^j ($\times 10^{-2}$)
1	-0.17626	3.24717	5	3.24717	-0.17626
2	-5.98282	2.91190	6	2.91190	-5.98282
3	2.91190	-5.98282	7	-5.98282	2.91190
4	3.24717	-0.17626	8	-0.17626	3.24717

Also, the shift invariant property of the CLL ensures that there is no temporal variation if we shift the initial conditions of each lattice point in the CML to its neighbour spatially. In this case, the wave pattern will also make only a corresponding shift.

Similarly, for the case of coupling force of period four, the evolution of the j^{th} map in the CML becomes

$$\begin{aligned} x_{n+1}^j &= f(x_n^j) + k_1^j, & x_{n+2}^j &= f(x_{n+1}^j) + k_2^j, \\ x_{n+3}^j &= f(x_{n+2}^j) + k_3^j, & x_{n+4}^j &= f(x_{n+3}^j) + k_4^j. \end{aligned} \quad (16)$$

The corresponding values of amplitudes of coupling force calculated as in the previous case are given in Table III. As before the coupling force oscillates with period four so as to form two standing waves [cf. Fig. 2(b)]. It may

also be noted that the amplitudes of the coupling force are decreasing with the increase of period.

TABLE III: Amplitudes of the coupling force k_1 , k_2 , k_3 and k_4 in the coupled map lattices for $L = 8$ with period-4 for the initial conditions, $\{x_0^j\}_{j=0}^{L-1} = \{0.0004, 0.0001, 0.0003, 0.0005, 0.00045, 0.00018, 0.00016, 0.00001\}$.

lattice site(j)	k_1^j ($\times 10^{-3}$)	k_2^j ($\times 10^{-3}$)	k_3^j ($\times 10^{-3}$)	k_4^j ($\times 10^{-3}$)
1	-6.26947	9.61098	1.03111	-2.92236
2	1.03111	-2.92235	-6.26947	9.61097
3	6.59582	-13.13797	-1.35746	6.44935
4	6.59582	-13.13797	-1.35746	6.44935
5	1.03111	-2.92236	-6.26947	9.61097
6	-6.26947	9.61097	1.03111	-2.92235
7	-1.35746	6.44935	6.59582	-13.13797
8	-1.35746	6.44935	6.59582	-13.13797

So, if it is possible to control the coupling force to fall in the region which corresponds to a periodic solution, then one can obtain standing wave patterns irrespective of the size of the lattices. This is in fact possible by choosing appropriate initial conditions to each lattice point and this explains the occurrence of standing waves (asynchronous) as shown in Figs. 2(a) and 2(b) in the CLL well below the critical lattice size (L_c). Similar explanation holds good for Fig. 2(c). The same principle is involved in the occurrence of standing waves even for $L > L_c$.

V. ANALYTICAL EXPRESSION FOR STANDING WAVE PATTERNS IN TERMS OF UPOs

In the previous section, we have seen that the amplitudes of the coupling force are decreasing while there is an increase in its period (p) of oscillation. For example, in the case of CLL, the forcing amplitudes, k_i^j , where $i = 1, 2, \dots, p$, is of the order of 10^{-2} for period-2, 10^{-3} for period-4, 10^{-4} for period-8 and so on. This implies that there is a possibility for the modified maps (at least some of the modified maps which have very weak coupling force) to nearly approach the original (unperturbed) map, since the perturbation (k_i^j) tends to zero for its higher periodic oscillations. So it is possible to approximately equate the fixed points of the modified map with the unstable periodic orbits (UPO) of the original constituent map of the CLL with its own parameter. Interestingly, it has been found from a careful numerical analysis that the nodes and antinodes of standing waves are formed at or very close to the UPOs of the isolated logistic map. It has also been noted that if nodes are at UPOs of period p then antinodes are at UPOs of period $2p$ of the isolated logistic map. Keeping this in mind, we propose an expression for the standing wave pattern [22]

of the form

$$x^j = u_k + A_k \sin \left(\frac{m\pi(j-\delta)}{L} \right) \cos(\pi i), \quad (17)$$

where,

$$A_k = \begin{cases} A_k^{\max}, & \text{if } \sin \left(\frac{m\pi(j-\delta)}{L} \right) \cos(\pi i) > 0 \\ A_k^{\min}, & \text{if } \sin \left(\frac{m\pi(j-\delta)}{L} \right) \cos(\pi i) < 0 \end{cases}$$

where the discrete index $j = 0, 1, 2, \dots, L-1$ corresponds to the lattice site, m denotes the mode of the waves, and k and i represent the nodes and antinodes of different standing waves present in the pattern, which can take values from 1 to p and 1 to $2p$, respectively. Also in the above equation (17), u_k 's represent the values of the UPOs of the isolated logistic map at the node of the k^{th} standing wave, and A_k^{\max} and A_k^{\min} are the absolute values of the differences between UPOs at the node and UPOs at high and low amplitudes at the antinodes of the k^{th} standing waves, respectively. One can easily calculate

TABLE IV: UPOs of the logistic map (14) for $\mu = 3.5732$.

period	unstable periodic orbit
1	0.72014
2	0.41337, 0.86649
4	0.35327, 0.53565, 0.81637, 0.88876
8	0.34317, 0.37614, 0.48393, 0.56000, 0.80542, 0.83848, 0.88044, 0.89238
16	0.84279, 0.56413, 0.89298, 0.34149, 0.50950, 0.34765, 0.80352, 0.36454, 0.87861, 0.47343, 0.38111, 0.82773, 0.54911, 0.81036, 0.88468, 0.89078

the UPOs of the logistic map (14) using Diakonos et al algorithm [23, 24]. The UPOs of the logistic map with the parameter $\mu = 3.5732$ for different periods are listed in Table IV. The advantage of this algorithm is that it can be used to find the unstable periodic orbits of very high periods.

The wave patterns with one and two number of standing waves obtained using Eq. (17) for $L = 8$ are shown in Fig. 4, whereas for the same lattice size, the numerically obtained pattern which have been discussed in section III is shown in Figs. 2(a) and 2(b). One observes that these two figures coincide very closely. Similarly, the numerically obtained standing wave patterns (with two different initial conditions) for the lattice size 15 is shown in Fig. 5, and for the same lattice size, the standing wave patterns obtained using period *four* (*eight*) and *eight* (*sixteen*) UPO at the nodes (antinodes), using the analytical form (17), are shown in Fig. 6. From these figures, it is observed that the standing wave patterns obtained by Eq. (17) is very nearly equivalent to the numerically obtained one if the number of standing waves is higher and atleast it is possible to predict the qualitative

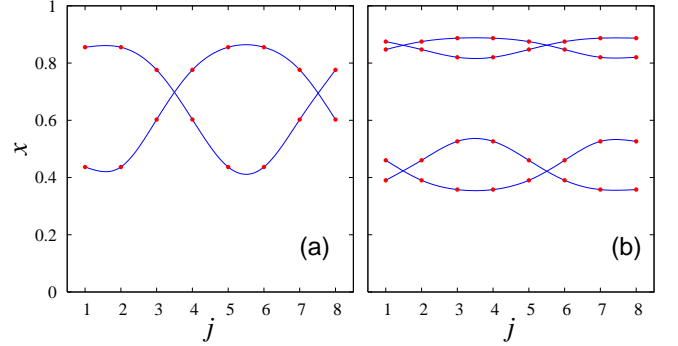


FIG. 4: Standing wave patterns obtained from Eq. (17) for $L = 8$: (a) standing wave with period-1 UPO at nodes and period-2 UPO at antinodes and (b) period-2 UPO at nodes and period-4 UPO at antinodes.

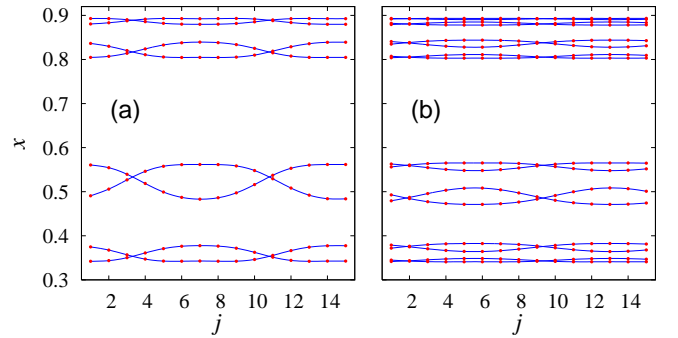


FIG. 5: Dynamics of coupled logistic lattice (1) and (14) with $L = 15$ for different initial conditions (a) four standing waves and (b) eight standing waves, obtained by numerical analysis.

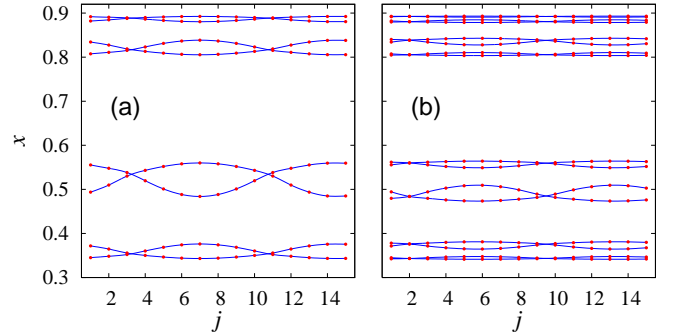


FIG. 6: Standing wave pattern obtained from Eq. (17) for $L = 15$ (a) standing wave with period-4 UPO at nodes and period-8 UPO at antinodes and (b) period-8 UPO at nodes and period-16 UPO at antinodes.

nature in the case of lower number standing waves in the pattern. Also it is noted that the standing waves are oscillating nearly about UPOs of period p at the node with the restriction that UPOs of period $2p$ are occupied at the antinodes. As a consequence of this property, there is

a deformation in the standing waves, that is, A_k^{max} and A_k^{min} are in general not the same.

VI. SUMMARY AND CONCLUSION

In summary, in the present paper, we have investigated the nature of size instability that occur in coupled map lattices. More importantly, we have pointed out that coupled map lattices exhibit multiple stable states for the same set of parameters with respect to the initial conditions. It has also been shown that by choosing appropriate initial conditions, one can obtain different standing wave type patterns for the coupled map lattices even for lattice size much less than the critical system size L_c , where one normally would expect synchronized chaos. We have traced the reason for the occurrence of such standing wave patterns as due to the nature of the coupling force and unstable periodic orbits of the isolated maps. Finally, we have given an analytic expression for the standing waves that arise in the CML. We have also extended the above analysis to coupled oscillators such as Rössler and nonlinear electronic circuits where also a similar phenomena occurs. Details will be published elsewhere.

Acknowledgments

This work has been supported by the National Board for Higher Mathematics, Department of Atomic Energy,

Government of India and the Department of Science and Technology, Government of India through research projects.

APPENDIX A: PHASE DIAGRAM

The phase diagram shown in Fig. 3 is drawn as follows. Consider a logistic map with an external periodic force of period-2 and it can be written as,

$$x_n = \mu x_{n-1}(1 - x_{n-1}) + \epsilon(n), \quad (A1)$$

where,

$$\epsilon(n) = \begin{cases} k_1 & \text{if } n \text{ is odd} \\ k_2 & \text{if } n \text{ is even} \end{cases}$$

and k_1 and k_2 are constants. For a random initial condition, the dynamics of this map is studied for different values of k_1 and k_2 in the range -0.1 to 0.1 with $\mu = 3.5732$. The values of k_1 and k_2 for which the map (A1) admits period-2 fixed point solution are noted and they are shown in Fig. 3.

[1] M. Lakshmanan and K. Murali, *Chaos in Nonlinear Oscillators: Controlling and Synchronization* (World Scientific, Singapore, 1996).

[2] A. Pikovsky, M. Rosenblum, and J. Kurths, *Synchronization: A Universal Concept in Nonlinear Sciences* (Cambridge University Press, Cambridge, 2001).

[3] M. Lakshmanan and S. Rajasekar, *Nonlinear Dynamics: Integrability, Chaos and Patterns* (Springer-Verlag, New York, 2003).

[4] P. Muruganandam, K. Murali, and M. Lakshmanan, Int. J. Bifur. Chaos: Appl. Sci. Eng. **9**, 805 (1999).

[5] P. Muruganandam and M. Lakshmanan, *Size instability and chaos synchronization in one dimensional array of diffusively coupled nonlinear oscillators* (2005), unpublished.

[6] H. Fujisaka and T. Yamada, Prog. Theor. Phys. **69**, 32 (1983).

[7] H. Fujisaka and T. Yamada, Prog. Theor. Phys. **70**, 1240 (1983).

[8] L. M. Pecora and T. L. Carroll, Phys. Rev. Lett. **64**, 821 (1990).

[9] K. Kaneko, *Collapse of Tori and Genesis of Chaos in Dissipative Systems* (World Scientific, Singapore, 1986).

[10] P. G. Lind, J. Corte-Real, and J. A. C. Gallas, Phys. Rev. E **66**, 016219 (2002).

[11] G. Francisco and P. Muruganandam, Phys. Rev. E **67**, 066204 (2003).

[12] K. Kaneko and I. Tsuda, *Complex Systems: Chaos and Beyond* (Springer, Berlin, 2000).

[13] T. Bohr and O. B. Christensen, Phys. Rev. Lett. **63**, 2161 (1989).

[14] J. F. Heagy, T. L. Carroll, and L. M. Pecora, Phys. Rev. E **50**, 1874 (1994).

[15] L. M. Pecora and T. L. Carroll, Phys. Rev. Lett. **80**, 2109 (1998).

[16] J. G. Restrepo, E. Ott, and B. R. Hunt, Phys. Rev. Lett. **93**, 114101 (2004).

[17] G. Rangarajan and M. Ding, Phys. Lett. A **296**, 204 (2002).

[18] Y. Chen, G. Rangarajan, and M. Ding, Phys. Rev. E **67**, 026209 (2003).

[19] A. V. Oppenheim and W. Schafer, *Discrete-Time Signal Processing* (Prentice-Hall, Englewood Cliffs, NJ, 1989).

[20] A. Venkatesan, S. Parthasarathy, and M. Lakshmanan, Chaos, Solitons and Fractals, **18**, 891 (2003).

[21] P. Palaniyandi and M. Lakshmanan, *Estimation of system parameters in discrete dynamical systems from time series* (2004), arXiv: nlin/0403058.

[22] I. G. Main, *Vibrations and Waves in Physics* (Cambridge University Press, Cambridge, 1993), 3rd ed.

- [23] F. K. Diakonos, P. Schmelcher, and O. Biham, Phys. Rev. Lett. **81**, 4349 (1998).
- [24] D. Pingel, P. Schmelcher, and F. K. Diakonos, Phys. Rep. **400**, 67 (2004).